

Method to Quantify the Black Carbon Aerosol Light Absorption Enhancement with ~~Entropy~~ ~~and Diversity Measures~~ Mixing State Index

Gang Zhao¹, Tianyi Tan¹, Yishu Zhu¹, Min Hu¹, Chunsheng Zhao^{2*}

¹ State Key Joint Laboratory of Environmental Simulation and Pollution Control, International Joint Laboratory for Regional Pollution Control, Ministry of Education, College of Environmental Sciences and Engineering, Peking University, Beijing, 100871, China

² Department of Atmospheric and Oceanic Sciences, School of Physics, Peking University, Beijing, 100871, China

*Correspondence author: Chunsheng Zhao (zcs@pku.edu.cn)

Abstract

Large uncertainties remain when estimating the warming effects of ambient black carbon (BC) aerosols on climate. One of the key challenges in modeling the radiative effects is predicting the BC light absorption enhancement, which is mainly determined by ~~its-the~~ mass ratio of non-BC coating ~~thickness-material~~ to BC in the population of BC-containing aerosols (MR). For the same MR, recent researches find that the radiative absorption enhancements by BC are also controlled by its particle-to-particle heterogeneity. In this study, the BC mixing state index (χ) is developed to quantify the dispersion of ambient black carbon aerosol mixing states based on binary systems of BC and other non-black carbon components. We demonstrate that the BC light absorption enhancement increases with χ for the same MR, which indicates that χ can be employed as a factor to constrain the light absorption enhancement of ambient BC. Our framework can be further used in the model to study the black carbon radiative effects on climate change.

1 Introduction

Black carbon (BC) aerosols absorb solar radiation, thus exert warming effects on the earth's energy system (Bond and Bergstrom, 2006; Bond et al., 2013). However, large uncertainties remain when quantifying the BC warming effects (Cui et al., 2016; Jacobson, 2010; Koch et al., 2009; Menon et al., 2002). Most of the BC particles were emitted from incomplete combustion of ~~bio-bio~~-fossil

28 fuel (Bond et al., 2013). After initially emitted, the BC particles would experience aging processing
29 with some other non-BC components coated on the BC particles (Peng et al., 2017;Peng et al., 2016).
30 During the aging processing, the light absorption of BC aerosols would increase, which is well
31 known as “lensing effects” (Saleh et al., 2013;Saleh et al., 2014). One critical challenge in estimating
32 the BC warming effects is quantifying the “lensing effects” of ambient BC aerosols (Liu et al., 2017).

33 The light absorption enhancement (E_{abs}), which is the ratio of light absorption of BC aerosols
34 with the coating to that of bare BC particles, is proposed to quantify the “lensing effects”.
35 Comprehensive studies have been carried out to study the E_{abs} (Liu et al., 2017;Peng et al.,
36 2016;Liu et al., 2015;Fierce et al., 2016;Fierce et al., 2020;Cappa et al., 2012). However, a large
37 discrepancy remains between the results of E_{abs} from field measurements and laboratory studies.
38 The measured E_{abs} of laboratory generated monodisperse BC particles can reach up to a factor of 2,
39 which is consistent with the results from the Mie scattering model (Cappa et al., 2012;Cappa et al.,
40 2019). However, some field measurement shows that the E_{abs} of ambient BC aerosols are relatively
41 small, with 1.06 at California (Cappa et al., 2012), 1.07 in South China (Lan et al., 2013), and 1.10 in
42 Japan (Nakayama et al., 2014), while the measured E_{abs} of ambient BC reaches 1.59 during
43 summer time in Beijing (Xie et al., 2019).

44 Many factors, such as the morphology of the BC core, the position of BC core inside coating, the
45 coating thickness, chemical properties of coating materials, and size distribution of the BC, would
46 influence the E_{abs} of ambient BC aerosols. Wu et al. (2018) reported that the BC light absorption
47 properties vary significantly for different morphology from the calculation of models. Laboratory
48 studies also find that the light absorption properties of the BC core were tuned due to the change of
49 the BC core morphology (Yuan et al., 2020). Comparing with the concentric spherical structure, the
50 off-center coated BC aggregates would lead to up to a 31% reduction in E_{abs} by the multiple-sphere
51 T-matrix method (Zhang et al., 2017). It has been well studied that the E_{abs} is highly related with
52 the mass ratio of coating materials and BC core (MR) (Liu et al., 2014;Liu et al., 2017). The coating
53 material are also critical in regulating the morphology and optical properties as the coating of sulfuric
54 acid has been shown to be more efficient in altering the BC morphology and light absorption(Zhang

55 | et al., 2008;Xue et al., 2009b, a). Zhao et al. (2019b) reported that the light absorption properties of
56 | ambient BC particles are influenced by BC mass size distribution. Besides, recently researchers
57 | found that the E_{abs} are also controlled by particle-to-particle heterogeneity (Fierce et al.,
58 | 2016;Fierce et al., 2020). As shown in Fig.1, the E_{abs} of ambient aerosols for the same MR would
59 | vary by about 30%, which is consistency with the results of Fierce et al. (2020). However, there is no
60 | study, to our best knowledge, that constrains the uncertainties of the E_{abs} for the same MR.

61 | In this study, we developed a BC mixing states index (χ) to quantify the dispersion of black
62 | carbon aerosol mixing states based on binary systems of BC and other non-black carbon components.
63 | We demonstrate that the BC E_{abs} increases with χ for the same MR based on the field measurement,
64 | which indicates that χ can be employed as a factor to constrain the E_{abs} properties of ambient BC.

65 | **2 Data and methods**

66 | **2.1 Field measurement**

67 | The field measurements were conducted at a suburban site Taizhou (119°57' E, 32°35' N) from
68 | 26 May to 18 June. As shown in Fig. S1, the Taizhou site lies between two large cities of Nanjing
69 | and Shanghai, where the aerosols can be seen as representative that of the Yangtze River Delta area
70 | (Liu et al., 2020). More details of the field measurements can refer to Zhao et al. (2019a). During the
71 | field measurement, we placed all of the instruments in a container where the temperature was
72 | carefully controlled between 22 and 26 °C. A PM₁₀ impactor, which is about 5 meters above the
73 | ground, was mounted on the top of the container. The sample aerosols were drawn from the impactor
74 | and then dried by a Nafion dryer tube.

75 | The size-resolved BC ~~mixing-states~~ score distribution and non-BC coating thickness were
76 | measured by using a differential mobility analyzer (DMA, model 3081, TSI, USA) in tandem with a
77 | single-particle soot photometer (SP2, Droplet Measurement Technologies, USA). Detailed
78 | information on the DMA can refer to Zhao et al. (2019c). SP2 can measure the BC mass
79 | concentration from the incandescence signals emitted by the BC particle, which is heated to around
80 | 6000 K by laser with a wavelength of 1064 nm (Zhao et al., 2020b). Along with the measurement of
81 | size-resolved BC ~~mixing-states~~ distributions, a nephelometer (Aurora 300, Ecotech, Australia)

82 (Müller et al., 2011) was employed to measure the aerosol scattering coefficient (σ_{sca}) at the
83 wavelength of 525 nm.

84 2.2 BC mixing states from DMA-SP2 system

85 In this study, the SP2 was placed after the DMA to measure the size-selected distribution of
86 BC-core and non-BC coating thickness mixing states of the quasi-monodisperse aerosols. The
87 schematic instrument setup is shown in Fig. S1 and the details can refer to part 1 in the
88 supplementary material. After careful calibrations of the SP2 (part 2.1 in the supplementary material),
89 transformations of the measured signals to BC mass concentrations (part 2.2 in the supplementary
90 material), and multiple charging corrections (part 2.3 in the supplementary material), the
91 BC-containing number concentration distribution under different total diameter (D_p) and BC core
92 diameter (D_c) can be calculated, as shown in Fig. S4 (b). The details of the calculation of
93 size-resolved distribution of BC mixing states core and coating thickness from the DMA-SP2 system
94 can refer to Zhao et al. (2020a). The measured size-resolved distribution of BC mixing states core and
95 coating thickness as in Fig. S4(b) were used for further analysis. It should be mentioned that the
96 measured number distribution of BC-containing aerosols is two dimensional ($\frac{d^2N}{d\log D_p \cdot d\log D_c} \frac{dN}{d\log D_p \cdot d\log D_c}$).
97 As noted by Zhao et al. (2020b), the SP2 can only detect these BC-containing aerosols with core
98 diameter larger than 84 nm. The DMA select the aerosol at the range between 13.3 nm and 749.9 nm.
99 In the following discussion, the size-resolved distribution of BC core and coating thickness are
100 constrained in the range between 84 and 749.9 nm.

101 2.3 Calculating the aerosol optical properties

102 2.3.1 Calculating the aerosol absorption coefficient for a given D_p and D_c

103 A Mie scattering model (Bohren and Huffman, 2007) was employed to calculate the aerosol
104 absorption coefficient (σ_{abs}). When calculating the σ_{abs} of single particle, the Mie scattering model
105 requires the diameter of the core, the coating thickness, the refractive index of the core, and the
106 refractive index of the shell. The refractive index of the core adopted here is $1.67+0.67i$, which is the
107 calculated mean value by comparing the measured light absorption and calculated light absorption
108 properties (Zhao et al., 2020a). The refractive index of the shell is chosen to be $1.46+0i$, which is

109 assumed to be as that of the non-BC component measured by the DMA-SP2 system (Zhao et al.,
 110 2019a; Zhao et al., 2019c). With the above information, the σ_{abs} values at a given D_p and a given D_c
 111 can be calculated.

112 2.3.2 Calculating the aerosol bulk absorption coefficient

113 We calculate the single-particle σ_{abs} of different D_p and D_c with the given refractive index of
 114 core and shell and then the ambient aerosol σ_{abs} distributions at different D_p and D_c
 115 ($\frac{d^2\sigma_{abs}}{d\log D_p \cdot d\log D_c} \frac{d\sigma_{abs}}{d\log D_p \cdot d\log D_c}$) can be calculated by multiplying the number concentrations of the
 116 BC-contained aerosols ($\frac{d^2N}{d\log D_p \cdot d\log D_c} \frac{dN}{d\log D_p \cdot d\log D_c}$). By integrating the $\frac{d^2\sigma_{abs}}{d\log D_p \cdot d\log D_c} \frac{d\sigma_{abs}}{d\log D_p \cdot d\log D_c}$ over
 117 different D_c values, the ambient aerosol σ_{abs} distribution along with different D_p ($\frac{d\sigma_{abs}}{d\log D_p}$) can be
 118 calculated. The total σ_{abs} of the ambient BC-containing aerosols can be calculated by integrating
 119 the $\frac{d\sigma_{abs}}{d\log D_p}$ over different D_p values.

120 2.3.3 Calculating the aerosol E_{abs}

121 Along with calculating the $\sigma_{abs, D_p, D_c} = \sigma_{abs}(D_p, D_c)$ of single-particle for different D_p and D_c ,
 122 we calculate the corresponding light absorption ($\sigma_{abs}(D_c, D_c) \sigma_{abs, D_c, D_c}$) value for D_c without
 123 thickness. The corresponding total light absorption of all measured BC-contained aerosols without-
 124 thicknesscoating can be calculated by integrating the calculated $\sigma_{abs}(D_c, D_c) \sigma_{abs, D_c, D_c}$ among
 125 different D_p and D_c weighted with $\frac{d^2N}{d\log D_p \cdot d\log D_c} \frac{dN}{d\log D_p \cdot d\log D_c}$. Thus the ambient BC particles without
 126 coating ($\sigma_{abs}(D_p = D_c) \sigma_{abs, D_p = \theta}$) can be calculated. The bulk ambient aerosol E_{abs} can thus be
 127 calculated with $E_{abs} = \frac{\sigma_{abs}}{\sigma_{abs}(D_p = D_c) \sigma_{abs, D_p = \theta}}$.

128 2.4 Quantifying the dispersion of BC mixing states

129 In this study, the mass-weighted mixing state index for BC-containing particles (χ) is developed
 130 to investigate the distribution of non-BC material across the BC-containing particle population,
 131 which is essentially the same as that of Yu et al. (2020). As for BC particles with known D_p and D_c ,
 132 the mass concentration of BC core and coating material can be calculated with the effective density
 133 of BC core and coating material. The effective density of the BC core is calculated in detail in
 134 section 2.2 in the supplement. The effective density of the coating material is assumed to be the same

135 as the measured effective density of non-BC aerosols by using a centrifugal particle mass analyzer
 136 (version 1.53, Cambustion Ltd, UK) in tandem with a scanning mobility particle sizer system (Zhao
 137 et al., 2019a) and a mean value of 1.5 g/cm³ was used here.

138 For each of the particle i ($i=1,2,\dots, N$ is the measured BC-containing aerosol number
 139 concentration), we can calculate its mass ratio of BC with

$$140 \quad p_{i,BC} = \frac{m_{i,BC}}{m_i}, \quad (1)$$

141 where $m_{i,BC}$ is the mass concentration of BC and m_i is the total mass concentration of particle i .

142 The mass portion of BC can be calculated as

$$143 \quad p_{BC} = \frac{m_{BC}}{m_{tot}}, \quad (2)$$

144 where m_{BC} (the total mass concentration of BC) and m_{tot} (total mass of BC-containing aerosols)

145 can be calculated as $m_{BC} = \sum_{i=1}^N m_{i,BC}$, $m_{tot} = \sum_{i=1}^N m_i$. The MR is calculated as:

$$146 \quad MR = \frac{(m_{tot}-m_{BC})}{m_{BC}}, \quad (3)$$

147 The mass portion of particle i to total BC-containing aerosols is calculated as

$$148 \quad p_i = \frac{m_i}{m_{tot}}. \quad (4)$$

149 With the definition above, we can calculate the mixing entropy of particle i (H_i) by:

$$150 \quad H_i = - (p_{i,BC} \ln(p_{i,BC}) + (1 - p_{i,BC}) \ln(1 - p_{i,BC})), \quad (5)$$

151 the average mixing entropy of ~~each particle~~the population by:

$$152 \quad H_\alpha = \sum_{i=1}^N p_i H_i, \quad (6)$$

153 And the population bulk mixing entropy by:

$$154 \quad H_\gamma = - (p_{BC} \ln(p_{BC}) + (1 - p_{BC}) \ln(1 - p_{BC})). \quad (7)$$

155 Then the average particle species diversity can be calculated by

$$156 \quad D_\alpha = e^{H_\alpha}, \quad (8)$$

157 And the bulk population species diversity can be calculated by

$$158 \quad D_\gamma = e^{H_\gamma}, \quad (9)$$

159 With the above information, the dispersion of BC particle mixing states can be defined as:

$$160 \quad \chi = \frac{D_\alpha - 1}{D_\gamma - 1}. \quad (10)$$

161 The basic idea of quantifying the BC particle mixing states is the same as that of Riemer and
162 West (2013) and Riemer et al. (2019), their framework mainly focuses on the bulk ambient aerosols
163 with about five species (Bondy et al., 2018;Ye et al., 2018). A number of different (binary) species
164 definitions for χ have been used in the literature. Ching et al. (2017) used this index to study the
165 impact of mixing of hygroscopic and non-hygroscopic species on cloud condensation nuclei. Dickau
166 et al. (2016) quantified the volatile and nonvolatile species mixing characters. Zheng et al. (2021)
167 compared three different variants for χ , one of which was based on absorbing (BC) and
168 non-absorbing species, and Yu et al. (2020) use a metric which is very related to this paper. ssOur
169 developed χ is a reduced parameter that only concerns the BC-containing aerosols with two species
170 of BC component and non-BC coating materials.

171 3. Results and Discussions

172 3.1 BC mixing states diagram

173 A mixing state diagram as shown in Fig. 2 was employed for better understanding the dispersion
174 of BC mixing states. Nine different ~~group bulks of~~ aerosols populations were given and summarized
175 in Table 1. For each group, we include six BC-containing particles with different mass
176 concentrations of BC core and non-BC coating material.

177 For group 1, the amounts of BC are very small (near zero) and most of the aerosols are
178 composed of the non-BC component. The D_α and D_γ values are 1.00 and 1.00 respectively. These
179 groups can also be described as all of the particles are pure BC particles without coating.

180 For groups 2, 3, and 4, the mass concentration ratios of the BC component to the non-BC
181 component are 1:5, 2:4, and 3:3 respectively. All of the D_α values are 1.00 for groups 2, 3, and 4
182 because the BC particles are externally mixed. The corresponding D_γ values are 1.56, 1.89, and
183 2.00 respectively. For these three groups, the χ values are all 0.00.

184 For groups 4, 5, 6, and 7, the mass concentration ratios of the BC component to the non-BC
185 component are all 1:1 while the BC component is mixed to a different extent. It is easy to conclude
186 that the BC particles of group 7 are most well mixed among these four groups. The corresponding χ
187 values are 0, 0.26, 0.83, and 1.0 for group 4, 5, 6, and 7, respectively.

188 As for groups 8 and 9, the mass concentration ratios of the BC component to the non-BC
189 component are 1:6.1. The D_γ values are 1.5 and the D_α values are 1.5 and 1.35 respectively.

190 From the different group, the average particle species diversity D_γ value is mainly determined
191 by the total mass concentration ratio of the BC component to the non-BC component. It varies
192 between 1 and 2 for different total mass concentration ratios. The D_γ increases when the mass ratio
193 approaches 1. The bulk population species diversity D_α ranges between 1 and D_γ . It denotes the
194 diversity of different BC-containing particles.

195 3.2 Overview of the measurement

196 Fig.S6 gives the time series of our field measurements results. During the field measurement, the
197 σ_{sca} varies between 29 and 1590 Mm^{-1} . The ranges of H_α , H_γ , D_α , D_γ , and χ are 0.10~0.55,
198 0.42~0.64, 1.32~1.72, 1.52~1.91 and 0.62~0.82 respectively.

199 For a better understanding of the characteristics of the above parameters, we only present the
200 time series of these parameters during a pollution period between 27, May and 30, May in Fig. 3. As
201 shown in Fig. 3, the MR increased from about 2 to 4 when the σ_{sca} increased from 300 to 1200
202 Mm^{-1} , which indicates that some secondary aerosol components were coated on the BC particles
203 when the ambient air is more polluted. During the aging processing, the H_α decreased from 0.51 to
204 0.38 and H_γ decreased from 0.63 to 0.49. The D_α decreases ~~with the MR~~ from 1.66 to 1.48. The
205 D_γ decreases with the MR from 1.86 to 1.66, which is consistent with the results in section 3.1 that
206 the $D_\gamma D_\alpha$ should decrease with the MR when the MR is larger than 1. The χ varies between 0.68
207 and 0.79. It is worth noting that the χ is not well correlated with the pollution conditions.

208 The daily variation of σ_{sca} , which is highly related to the development of the boundary layer,
209 reaches its maximum value of 525 Mm^{-1} at 6:00 AM and a minimum value of 150 Mm at 7:00 PM.
210 The daily variation of MR is largest at 5:00 AM with a mean value of 3.16 and reaches its minimum
211 value of 2.56 at 7:00 PM. The daily variation of MR was mainly influenced by aging processing and
212 anthropogenic activities. During the daytime, the newly emitted BC particles due to anthropogenic
213 activities have low MR and the measured mean MR is low than that at night. The D_α values, which
214 are anti-correlated with MR, show the opposite trend with MR. As for χ , it is smaller in the daytime

215 than that at night. The lower χ values at daytime mainly resulted from the mixing of newly emitted
216 BC particles due to anthropogenic activities and some pre-existed aged BC particles.

217 **3.3 Relationship between the χ and E_{abs} from measurement**

218 For each of the measured group of size-resolved ~~distribution of BC core and coating thickness~~
219 ~~BC mixing states~~, we calculated the corresponding MR, χ , and E_{abs} . And the relationship between the
220 MR and absorption enhancement is summarized in Fig. 5. It should be noted that the shown BC
221 population is only one of possible examples with χ equaling 0, 0.81, and 1 respectively. There are
222 many other possible ways the particle composition can be arranged that would give the same mixing
223 state index.

224 Overall, the BC E_{abs} increase with MR, which is consistent with the previous knowledge. For a
225 given value of MR, E_{abs} varies by about 20%, especially for these conditions with MR larger than
226 1.0. When MR is larger than 1.0, the E_{abs} increase with the χ . Relationship between the E_{abs} and χ
227 is rather complex when MR is smaller than 1.0. However, only 448 of 6948 groups (6.4%) of the
228 measured MR values are smaller than 1. Therefore, for most of the conditions, the measured E_{abs}
229 should increase with χ , which indicates that the ~~refractive index of~~BC mixing state index χ can be
230 employed as a factor to constrain the E_{abs} of ambient aerosols.

231 A schematic diagram as shown in Fig. 6 to denotes the relationship between the E_{abs} and χ .
232 From Fig. 6, we calculated the E_{abs} and χ under differ MR and then compared the E_{abs} of different
233 bulk aerosols. The first group contains two particles with both the MR equaling 8. The corresponding
234 χ is 1.00 and E_{abs} is 1.60. Another group of particles contains two particles with MR equaling 1 and
235 15, respectively. Thus the second group of particles has a mean MR of 8. The calculated
236 corresponding χ and E_{abs} are 0.79 and 1.42 respectively. Thus, the E_{abs} tend to increase with χ for
237 the same MR, which is mainly resulted from that the increasing ratio of E_{abs} (the slope of E_{abs} to
238 MR) decrease with MR.

239 It is worth noting that the increasing ratio is almost the same when the MR is in the range of 0
240 and 3. Therefore, the E_{abs} doesn't tend to increase with the χ when the MR was less than 1, which
241 is consistent with our study as shown in Fig. 6.

242 **3.4 Relationship between the χ and E_{abs} from simulation**

243 A Mont-Carlo simulation was carried out for a better understanding of the relationship between
244 χ and E_{abs} . During the simulation, the number of BC-containing particles was assumed to be 30. For
245 each of the BC particle, the core diameter of the BC particle was randomly generated with a
246 geometric mean diameter of 130.7 nm and a geometric standard deviation of 1.5, which is the mean
247 measurement results of the BC core distribution during the field measurement (Zhao et al., 2020b).
248 The corresponding MR of the BC particle is assumed to be in the range between 0.0 (pure BC
249 particles without coating) and 78.0 (particles with a core diameter of 130 nm and a total diameter of
250 560 nm). For each of the group of particles, the corresponding aerosol bulk MR, E_{abs} and χ can be
251 calculated. The simulations were conducted for 10^7 times, and the calculated mean and standard
252 deviation of E_{abs} under different MR and χ are summarized in Fig. 7 (a) and (b).

253 From Fig. 7 (a), the calculated E_{abs} tend to increase with MR for each of the given χ , which is
254 consistent with the previous knowledge of the BC light absorption properties. Then the MR is
255 smaller than 2, the calculated E_{abs} does not seem to increase with the χ , which is consistent with the
256 analyzed results from section 3.3 and Fig. 6. When the MR is larger 2, the E_{abs} tend to increase
257 with the χ . The larger the MR is, the E_{abs} is more sensitive to χ . Two reasons may lead to this
258 phenomenon. One reason is that that calculated slope of E_{abs} to MR for one particle as shown in Fig.
259 6 decreases with the MR. Another reason is that the calculated E_{abs} range increase with MR when
260 the χ changes between 0 and 1 as shown in Fig. 5.

261 As for the uncertainties of simulated E_{abs} , it tends to increase with the MR, which is consistent
262 with the previous discussions that the E_{abs} the range tends to increase with MR. Overall, the
263 calculated standard deviations of E_{abs} are all the way smaller than 10% for different MR and χ .
264 Therefore, the calculated E_{abs} can be well constrained by χ .

265 **4 Conclusion**

266 Larger uncertainties remain when estimating the warming effects of ambient BC aerosols due to
267 the poor understanding of the ambient BC light absorption enhance ratio. Previous studies find that
268 the light absorption of ambient aerosols was mainly determined by the morphology of the BC core,
269 the position of the BC core inside coating, the coating thickness, and the size distribution of the BC.

270 We find that there are more than 20% of uncertainties for the same measured mean coating thickness,
271 i.e. the same measured MR based on the field measurement of the size-resolved distribution of BC
272 core and coating thickness~~BC mixing states~~. However, there were no study, to our best knowledge,
273 that attempts to constrain the uncertainties.

274 In this study, we developed the BC mixing states index χ based on the mass concentrations of
275 BC components and non-BC material of each BC-containing particle. Results show that the light
276 absorption enhancement ratio E_{abs} tend to increase the χ for the same measured MR. Therefore, our
277 developed parameter χ , which reflects the dispersion of the BC mixing states, can be employed as an
278 effective parameter to constrain the light absorption enhancement of ambient BC-containing
279 aerosols.

280 The new finding of our study is ~~Our study offer new insight~~ that the mixing state
281 index can contribute to improvements in the accuracy of simulating the BC radiative
282 effects. In the particle-resolved simulation of ambient aerosols, the particle-to-particle
283 heterogeneity of BC-containing aerosols can be resolved by simply introduce the BC
284 mixing state index χ . Then the aerosol light absorption enhancement can be better
285 constrained by MR and χ and then the radiative effects of BC can be estimated.
286 Therefore, our framework can be employed in the model by simply introduce a BC
287 mixing state index for better estimating the BC radiative effects.

288
289 **Data availability.** The data involved is available in the manuscript.

290 **Author contributions.** Gang Zhao wrote the manuscript. Chunsheng Zhao, Min Hu, Tianyi Tan,
291 Song Guo, Zhijun Wu, Yishu Zhu and Gang Zhao discussed the results.

292 **Competing interests.** The authors declare that they have no conflict of interest.

293 **Acknowledgments.** This work is supported by the National Key R&D Program of China
294 (2016YFC020000: Task 5) and the National Natural Science Foundation of China (41590872).

295

296

297

298

299 Bohren, C. F., and Huffman, D. R.: Absorption and Scattering by a Sphere, in: Absorption and
300 Scattering of Light by Small Particles, Wiley-VCH Verlag GmbH, 82-129, 2007.

301 Bond, T. C., and Bergstrom, R. W.: Light Absorption by Carbonaceous Particles: An Investigative
302 Review, *Aerosol Sci. Technol.*, 40, 27-67, 10.1080/02786820500421521, 2006.

303 Bond, T. C., Doherty, S. J., Fahey, D. W., Forster, P. M., Berntsen, T., DeAngelo, B. J., Flanner, M.
304 G., Ghan, S., Karcher, B., Koch, D., Kinne, S., Kondo, Y., Quinn, P. K., Sarofim, M. C., Schultz, M.
305 G., Schulz, M., Venkataraman, C., Zhang, H., Zhang, S., Bellouin, N., Guttikunda, S. K., Hopke, P.
306 K., Jacobson, M. Z., Kaiser, J. W., Klimont, Z., Lohmann, U., Schwarz, J. P., Shindell, D.,
307 Storelvmo, T., Warren, S. G., and Zender, C. S.: Bounding the role of black carbon in the climate
308 system: A scientific assessment, *J Geophys Res-Atmos*, 118, 5380-5552, 10.1002/jgrd.50171, 2013.

309 Bondy, A. L., Bonanno, D., Moffet, R. C., Wang, B., Laskin, A., and Ault, A. P.: The diverse
310 chemical mixing state of aerosol particles in the southeastern United States, *Atmospheric Chemistry
311 and Physics*, 18, 12595-12612, 10.5194/acp-18-12595-2018, 2018.

312 Cappa, C. D., Onasch, T. B., Massoli, P., Worsnop, D. R., Bates, T. S., Cross, E. S., Davidovits, P.,
313 Hakala, J., Hayden, K. L., Jobson, B. T., Kolesar, K. R., Lack, D. A., Lerner, B. M., Li, S. M.,
314 Mellon, D., Nuaaman, I., Olfert, J. S., Petaja, T., Quinn, P. K., Song, C., Subramanian, R., Williams,
315 E. J., and Zaveri, R. A.: Radiative Absorption Enhancements Due to the Mixing State of
316 Atmospheric Black Carbon, *Science*, 337, 1078-1081, 10.1126/science.1223447, 2012.

317 Cappa, C. D., Zhang, X., Russell, L. M., Collier, S., Lee, A. K. Y., Chen, C.-L., Betha, R., Chen, S.,
318 Liu, J., Price, D. J., Sanchez, K. J., McMeeking, G. R., Williams, L. R., Onasch, T. B., Worsnop, D.
319 R., Abbatt, J., and Zhang, Q.: Light Absorption by Ambient Black and Brown Carbon and its
320 Dependence on Black Carbon Coating State for Two California, USA, Cities in Winter and Summer,
321 *Journal of Geophysical Research: Atmospheres*, 124, 1550-1577, 10.1029/2018jd029501, 2019.

322 Ching, J., Fast, J., West, M., and Riemer, N.: Metrics to quantify the importance of mixing state for
323 CCN activity, *Atmospheric Chemistry and Physics*, 17, 7445-7458, 10.5194/acp-17-7445-2017,
324 2017.

325 Cui, X., Wang, X., Yang, L., Chen, B., Chen, J., Andersson, A., and Gustafsson, Ö.: Radiative
326 absorption enhancement from coatings on black carbon aerosols, *Science of The Total Environment*,
327 551-552, 51-56, doi.org/10.1016/j.scitotenv.2016.02.026, 2016.

328 Dickau, M., Olfert, J., Stettler, M. E. J., Boies, A., Momenimovahed, A., Thomson, K., Smallwood,
329 G., and Johnson, M.: Methodology for quantifying the volatile mixing state of an aerosol, *Aerosol*
330 *Sci. Technol.*, 50, 759-772, 10.1080/02786826.2016.1185509, 2016.

331 Fierce, L., Bond, T. C., Bauer, S. E., Mena, F., and Riemer, N.: Black carbon absorption at the global
332 scale is affected by particle-scale diversity in composition, *Nature communications*, 7, 12361,
333 10.1038/ncomms12361, 2016.

334 Fierce, L., Onasch, T. B., Cappa, C. D., Mazzoleni, C., China, S., Bhandari, J., Davidovits, P.,
335 Fischer, D. A., Helgestad, T., Lambe, A. T., Sedlacek, A. J., 3rd, Smith, G. D., and Wolff, L.:
336 Radiative absorption enhancements by black carbon controlled by particle-to-particle heterogeneity
337 in composition, *Proceedings of the National Academy of Sciences of the United States of America*,
338 117, 5196-5203, 10.1073/pnas.1919723117, 2020.

339 Jacobson, M. Z.: Short-term effects of controlling fossil-fuel soot, biofuel soot and gases, and
340 methane on climate, Arctic ice, and air pollution health, *Journal of Geophysical Research:*
341 *Atmospheres*, 115, n/a-n/a, 10.1029/2009JD013795, 2010.

342 Koch, D., Schulz, M., Kinne, S., and Mcnaughton, C.: Evaluation of black carbon estimations in
343 global aerosol models, *Atmospheric Chemistry & Physics*, 9, 9001-9026, 2009.

344 Lan, Z.-J., Huang, X.-F., Yu, K.-Y., Sun, T.-L., Zeng, L.-W., and Hu, M.: Light absorption of black
345 carbon aerosol and its enhancement by mixing state in an urban atmosphere in South China,
346 *Atmospheric Environment*, 69, 118-123, 10.1016/j.atmosenv.2012.12.009, 2013.

347 Liu, D., Allan, J. D., Young, D. E., Coe, H., Beddows, D., Fleming, Z. L., Flynn, M. J., Gallagher, M.
348 W., Harrison, R. M., Lee, J., Prevot, A. S. H., Taylor, J. W., Yin, J., Williams, P. I., and Zotter, P.:
349 Size distribution, mixing state and source apportionment of black carbon aerosol in London during
350 wintertime, *Atmospheric Chemistry and Physics*, 14, 10061-10084, 10.5194/acp-14-10061-2014,
351 2014.

352 Liu, D., Whitehead, J., Alfarra, M. R., Reyes-Villegas, E., Spracklen, Dominick V., Reddington,
353 Carly L., Kong, S., Williams, Paul I., Ting, Y.-C., Haslett, S., Taylor, Jonathan W., Flynn, Michael J.,
354 Morgan, William T., McFiggans, G., Coe, H., and Allan, James D.: Black-carbon absorption
355 enhancement in the atmosphere determined by particle mixing state, *Nature Geoscience*, 10, 184-188,
356 10.1038/ngeo2901, 2017.

357 Liu, J., Li, X., Li, D., Xu, R., Gao, Y., Chen, S., Liu, Y., Zhao, G., Wang, H., Wang, H., Lou, S.,
358 Chen, M., Hu, J., Lu, K., Wu, Z., Hu, M., Zeng, L., and Zhang, Y.: Observations of glyoxal and
359 methylglyoxal in a suburban area of the Yangtze River Delta, China, *Atmospheric Environment*, 238,
360 117727, 10.1016/j.atmosenv.2020.117727, 2020.

361 Liu, S., Aiken, A. C., Gorkowski, K., Dubey, M. K., Cappa, C. D., Williams, L. R., Herndon, S. C.,
362 Massoli, P., Fortner, E. C., Chhabra, P. S., Brooks, W. A., Onasch, T. B., Jayne, J. T., Worsnop, D.
363 R., China, S., Sharma, N., Mazzoleni, C., Xu, L., Ng, N. L., Liu, D., Allan, J. D., Lee, J. D., Fleming,
364 Z. L., Mohr, C., Zotter, P., Szidat, S., and Prevot, A. S.: Enhanced light absorption by mixed source
365 black and brown carbon particles in UK winter, *Nature communications*, 6, 8435,
366 10.1038/ncomms9435, 2015.

367 Menon, S., Hansen, J., Nazarenko, L., and Luo, Y.: Climate effects of black carbon aerosols in China
368 and India, *Science*, 297, 2250-2253, 10.1126/science.1075159, 2002.

369 Müller, T., Laborde, M., Kassell, G., and Wiedensohler, A.: Design and performance of a
370 three-wavelength LED-based total scatter and backscatter integrating nephelometer, *Atmos. Meas.*
371 *Tech.*, 4, 1291-1303, 10.5194/amt-4-1291-2011, 2011.

372 Nakayama, T., Ikeda, Y., Sawada, Y., Setoguchi, Y., Ogawa, S., Kawana, K., Mochida, M., Ikemori,
373 F., Matsumoto, K., and Matsumi, Y.: Properties of light-absorbing aerosols in the Nagoya urban area,
374 Japan, in August 2011 and January 2012: Contributions of brown carbon and lensing effect, *Journal*
375 *of Geophysical Research: Atmospheres*, 119, 7211-7217, 10.1002/2014JD021744, 2014.

376 Peng, J., Hu, M., Guo, S., Du, Z., Zheng, J., Shang, D., Levy Zamora, M., Zeng, L., Shao, M., Wu,
377 Y.-S., Zheng, J., Wang, Y., Glen, C. R., Collins, D. R., Molina, M. J., and Zhang, R.: Markedly
378 enhanced absorption and direct radiative forcing of black carbon under polluted urban environments,

379 Proceedings of the National Academy of Sciences, 113, 4266-4271, 10.1073/pnas.1602310113,
380 2016.

381 Peng, J., Hu, M., Guo, S., Du, Z., Shang, D., Zheng, J., Zheng, J., Zeng, L., Shao, M., Wu, Y.,
382 Collins, D., and Zhang, R.: Ageing and hygroscopicity variation of black carbon particles in Beijing
383 measured by a quasi-atmospheric aerosol evolution study (QUALITY) chamber, Atmospheric
384 Chemistry and Physics, 17, 10333-10348, 10.5194/acp-17-10333-2017, 2017.

385 Riemer, N., and West, M.: Quantifying aerosol mixing state with entropy and diversity measures,
386 Atmospheric Chemistry and Physics, 13, 11423-11439, 10.5194/acp-13-11423-2013, 2013.

387 Riemer, N., Ault, A. P., West, M., Craig, R. L., and Curtis, J. H.: Aerosol Mixing State:
388 Measurements, Modeling, and Impacts, Reviews of Geophysics, 57, 187-249,
389 10.1029/2018rg000615, 2019.

390 Saleh, R., Hennigan, C. J., McMeeking, G. R., Chuang, W. K., Robinson, E. S., Coe, H., Donahue, N.
391 M., and Robinson, A. L.: Absorptivity of brown carbon in fresh and photo-chemically aged
392 biomass-burning emissions, Atmos. Chem. Phys., 13, 7683-7693, 10.5194/acp-13-7683-2013, 2013.

393 Saleh, R., Robinson, E. S., Tkacik, D. S., Ahern, A. T., Liu, S., Aiken, A. C., Sullivan, R. C., Presto,
394 A. A., Dubey, M. K., Yokelson, R. J., Donahue, N. M., and Robinson, A. L.: Brownness of organics
395 in aerosols from biomass burning linked to their black carbon content, Nature Geoscience, 7, 647,
396 10.1038/ngeo2220, 2014.

397 Wu, Y., Cheng, T., Liu, D., Allan, J. D., Zheng, L., and Chen, H.: Light Absorption Enhancement of
398 Black Carbon Aerosol Constrained by Particle Morphology, Environ Sci Technol, 52, 6912-6919,
399 10.1021/acs.est.8b00636, 2018.

400 Xie, C., Xu, W., Wang, J., Liu, D., Ge, X., Zhang, Q., Wang, Q., Du, W., Zhao, J., Zhou, W., Li, J.,
401 Fu, P., Wang, Z., Worsnop, D., and Sun, Y.: Light absorption enhancement of black carbon in urban
402 Beijing in summer, Atmospheric Environment, 10.1016/j.atmosenv.2019.06.041, 2019.

403 Xue, H., Khalizov, A. F., Wang, L., Zheng, J., and Zhang, R.: Effects of coating of dicarboxylic
404 acids on the mass-mobility relationship of soot particles, Environmental Science & Technology, 43,
405 2787-2792, 2009a.

406 Xue, H., Khalizov, A. F., Wang, L., Zheng, J., and Zhang, R.: Effects of dicarboxylic acid coating on
407 the optical properties of soot, *Physical Chemistry Chemical Physics*, 11, 7869-7875,
408 10.1039/B904129J, 2009b.

409 Ye, Q., Gu, P., Li, H. Z., Robinson, E. S., Lipsky, E., Kaltsonoudis, C., Lee, A. K. Y., Apte, J. S.,
410 Robinson, A. L., Sullivan, R. C., Presto, A. A., and Donahue, N. M.: Spatial Variability of Sources
411 and Mixing State of Atmospheric Particles in a Metropolitan Area, *Environ Sci Technol*, 52,
412 6807-6815, 10.1021/acs.est.8b01011, 2018.

413 Yu, C., Liu, D., Broda, K., Joshi, R., Olfert, J., Sun, Y., Fu, P., Coe, H., and Allan, J. D.:
414 Characterising mass-resolved mixing state of black carbon in Beijing using a
415 morphology-independent measurement method, *Atmospheric Chemistry and Physics*, 20, 3645-3661,
416 10.5194/acp-20-3645-2020, 2020.

417 Yuan, C., Zheng, J., Ma, Y., Jiang, Y., Li, Y., and Wang, Z.: Significant restructuring and light
418 absorption enhancement of black carbon particles by ammonium nitrate coating, *Environ Pollut*, 262,
419 114172, 10.1016/j.envpol.2020.114172, 2020.

420 Zhang, R., Khalizov, A. F., Pagels, J., Zhang, D., Xue, H., and McMurry, P. H.: Variability in
421 morphology, hygroscopicity, and optical properties of soot aerosols during atmospheric processing,
422 *Proceedings of the National Academy of Sciences of the United States of America*, 105,
423 10291-10296, 10.1073/pnas.0804860105, 2008.

424 Zhang, X., Mao, M., Yin, Y., and Wang, B.: Absorption enhancement of aged black carbon aerosols
425 affected by their microphysics: a numerical investigation, *Journal of Quantitative Spectroscopy and
426 Radiative Transfer*, 202, 90-97, 10.1016/j.jqsrt.2017.07.025, 2017.

427 Zhao, G., Tan, T., Zhao, W., Guo, S., Tian, P., and Zhao, C.: A new parameterization scheme for the
428 real part of the ambient urban aerosol refractive index, *Atmos. Chem. Phys.*, 19, 12875-12885,
429 10.5194/acp-19-12875-2019, 2019a.

430 Zhao, G., Tao, J., Kuang, Y., Shen, C., Yu, Y., and Zhao, C.: Role of black carbon mass size
431 distribution in the direct aerosol radiative forcing, *Atmos. Chem. Phys.*, 19, 13175-13188,
432 10.5194/acp-19-13175-2019, 2019b.

433 Zhao, G., Zhao, W., and Zhao, C.: Method to measure the size-resolved real part of aerosol refractive
434 index using differential mobility analyzer in tandem with single-particle soot photometer,
435 Atmospheric Measurement Techniques, 12, 3541-3550, 10.5194/amt-12-3541-2019, 2019c.

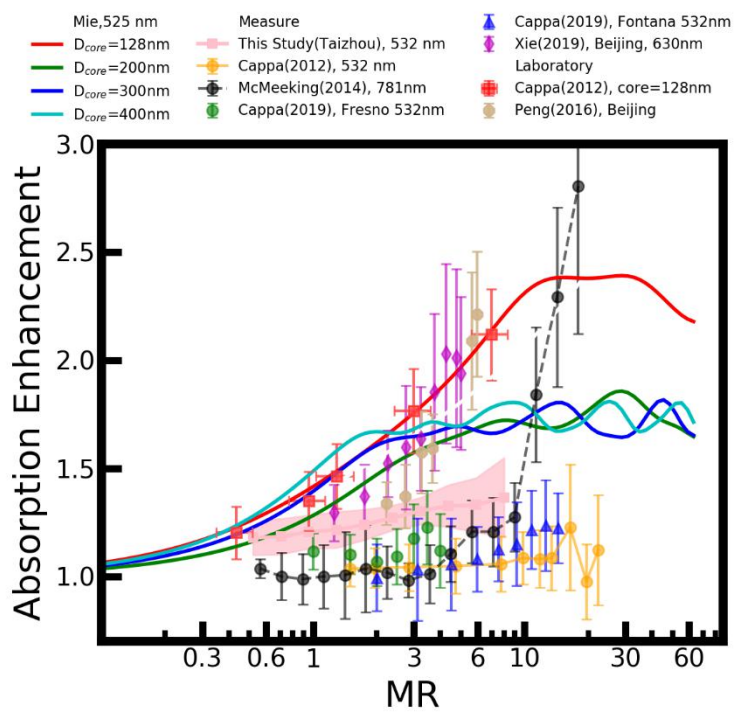
436 Zhao, G., Li, F., and Zhao, C.: Determination of the refractive index of ambient aerosols,
437 Atmospheric Environment, 240, 117800, 10.1016/j.atmosenv.2020.117800, 2020a.

438 Zhao, G., Shen, C., and Zhao, C.: Technical note: Mismeasurement of the core-shell structure of
439 black carbon-containing ambient aerosols by SP2 measurements, Atmospheric Environment, 243,
440 117885, 10.1016/j.atmosenv.2020.117885, 2020b.

441 Zheng, Z., Curtis, J. H., Yao, Y., Gasparik, J. T., Anantharaj, V. G., Zhao, L., West, M., and Riemer,
442 N.: Estimating Submicron Aerosol Mixing State at the Global Scale With Machine Learning and
443 Earth System Modeling, Earth and Space Science, 8, 10.1029/2020ea001500, 2021.

444

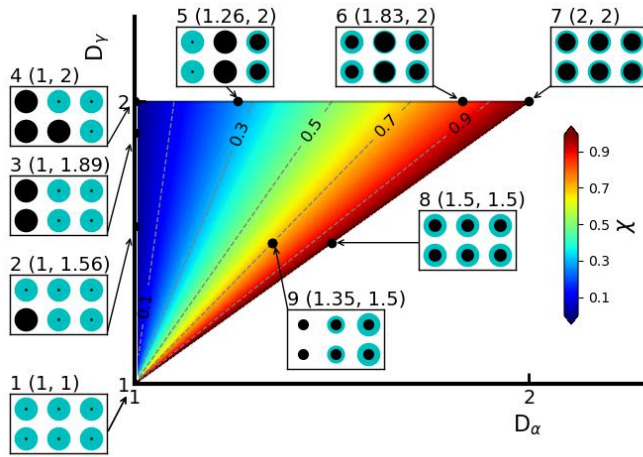
445



446

447 Figure 1. The measured E_{abs} of BC particles from different ambient measurements, including this
 448 work (in pink), and lab studies.

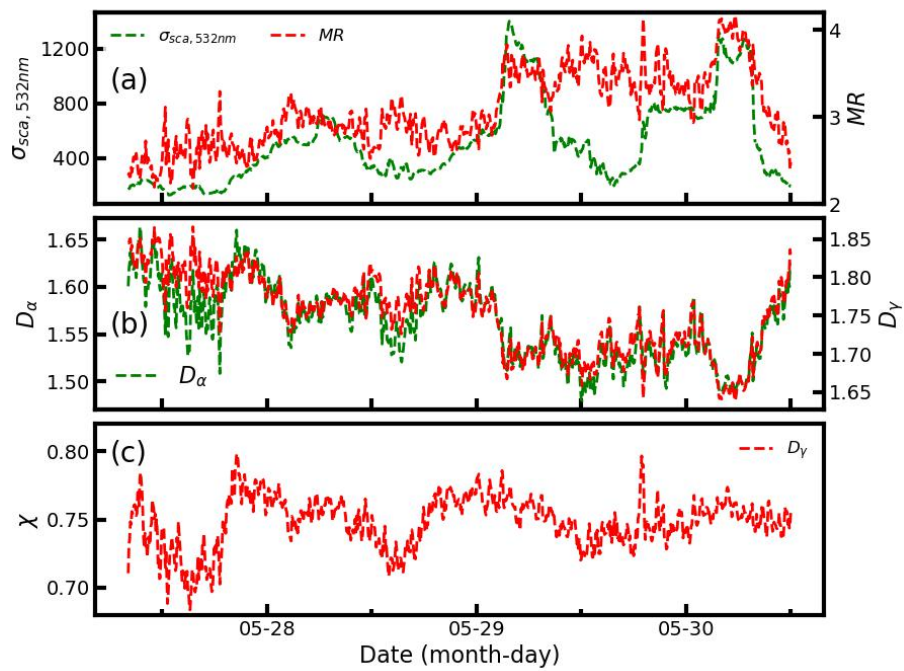
449



450

451 **Figure 2.** Mixing states diagram to illustrate the relationship between D_α , D_γ , and χ . Each species
 452 consists of six particles, and the colors of black and cyan represent the BC and non-BC components.

453

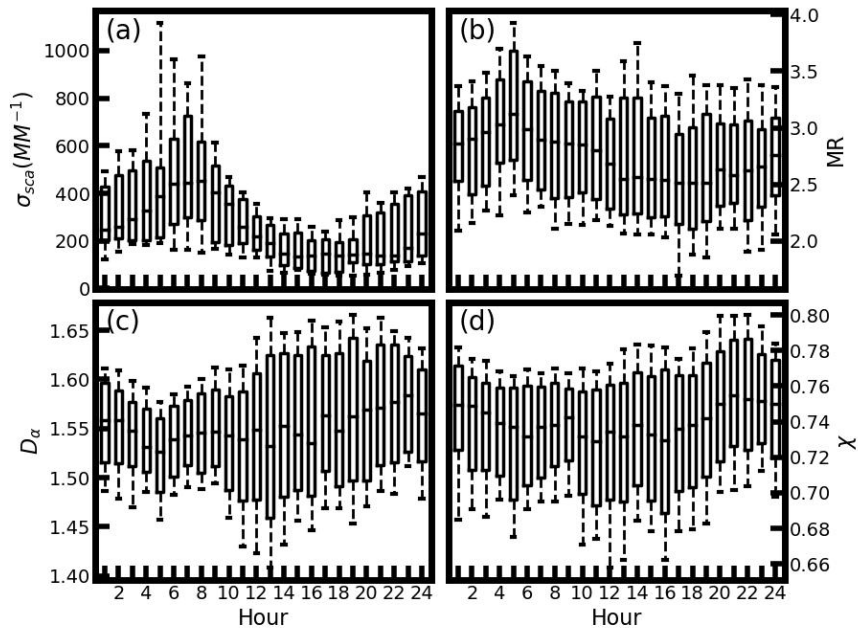


454

455

Figure 3. Measured time series of (a) σ_{sca} and MR, (b) H_{α} and H_{γ} , (c) D_{α} and D_{γ} , and (d) χ .

456

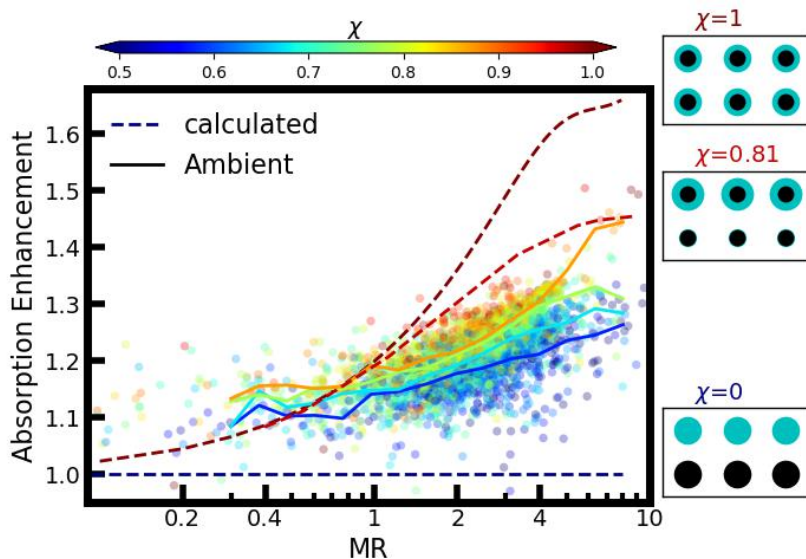


457

458 **Figure 4.** Daily variation of the measured (a) σ_{sca} , (b) MR, (c) D_α , and (d) χ .

459

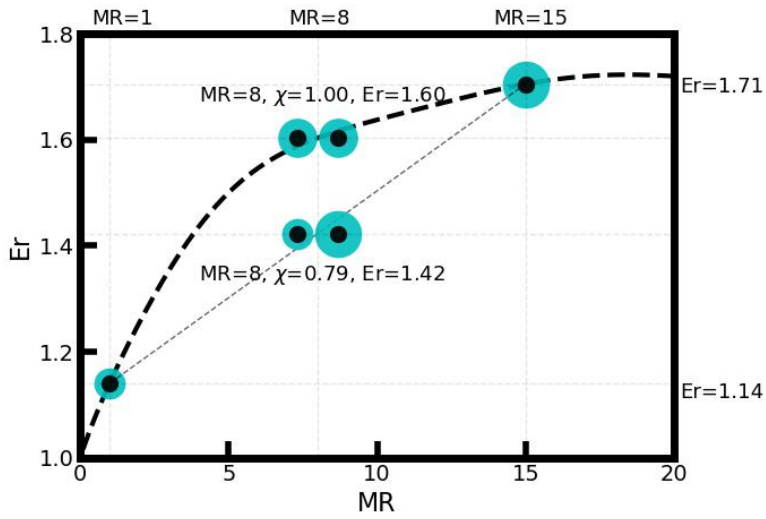
460



461

462 **Figure 5.** Relationship between the BC E_{abs} and the measured mass ratio of the BC-containing
 463 aerosols coating material to BC under different χ conditions. Four solid lines from bottom to up
 464 corresponding to the measured ambient size-resolved BC mixing states data with χ ranges of
 465 0.575~0.625, 0.625~0.675, 0.675~0.725, and 0.725~0.775. The dotted line corresponds to the χ of
 466 0.0 (blue), 0.81 (light red), and 1.0 (dark red), respectively.

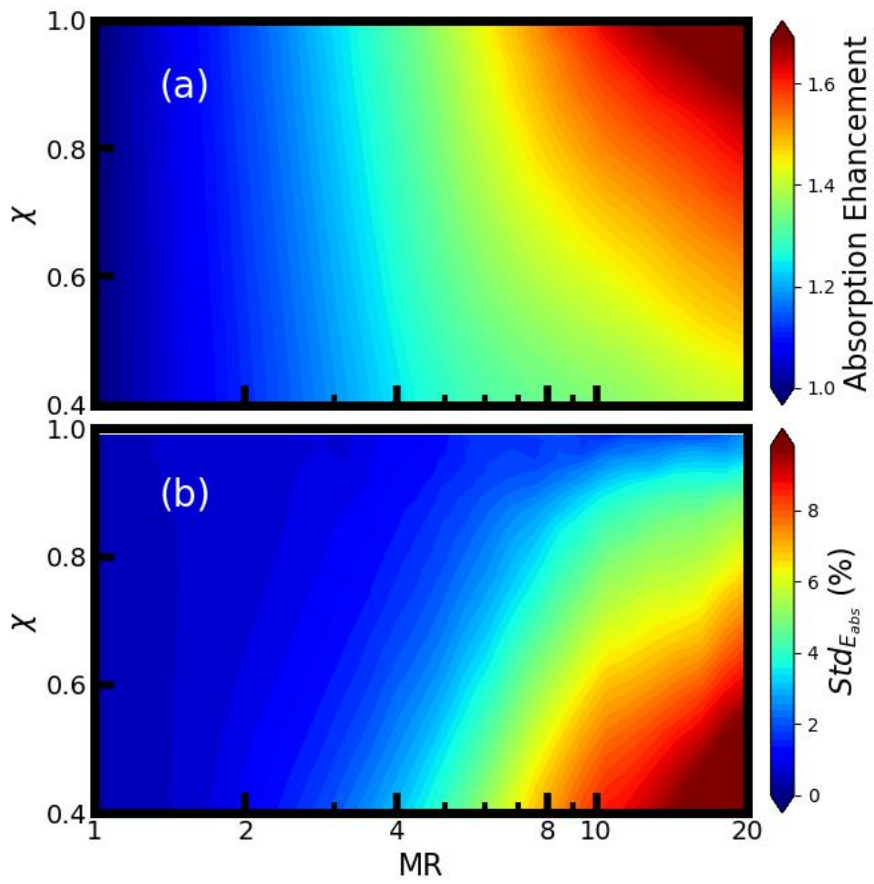
467



468

469 **Figure 6.** Schematic diagram that denotes the relationship between χ and E_r .

470



471

472 **Figure 7.** The calculated (a) mean E_{abs} values and (b) standard deviations of the E_{abs} values for
 473 different MR and χ .

ID	(D_α, D_γ)	χ	P1 ^{*1}	P2 ^{*1}	P3 ^{*1}	P4 ^{*1}	P5 ^{*1}	P6 ^{*1}	Tot ^{*1}
1	(1.00, 1.00)	-	(10 ⁻⁹ ,1)	(10 ⁻⁹ ,1)	(10 ⁻⁹ ,1)	(10 ⁻⁹ ,1)	(10 ⁻⁹ ,1)	(10 ⁻⁹ ,1)	(6 ·10 ⁻⁹ ,1)
2	(1.00,1.56)	0	(1,10 ⁻⁹)	(10 ⁻⁹ , 1)	(10 ⁻⁹ , 1)	(10 ⁻⁹ , 1)	(10 ⁻⁹ , 1)	(10 ⁻⁹ , 1)	(1, 5)
3	(1.00, 1.89)	0	(1,10 ⁻⁹)	(1,10 ⁻⁹)	(10 ⁻⁹ , 1)	(10 ⁻⁹ , 1)	(10 ⁻⁹ , 1)	(10 ⁻⁹ , 1)	(2,4)
4	(1.00, 2.00)	0	(1,10 ⁻⁹)	(1,10 ⁻⁹)	(1,10 ⁻⁹)	(10 ⁻⁹ , 1)	(10 ⁻⁹ , 1)	(10 ⁻⁹ , 1)	(3,3)
5	(1.26, 2.00)	0.26	(2,10 ⁻⁹)	(2,10 ⁻⁹)	(10 ⁻⁹ ,2)	(10 ⁻⁹ ,2)	(10 ⁻⁹ ,1)	(1,1)	(6, 6)
6	(1.83, 2.00)	0.83	(1,3)	(1,3)	(3,1)	(3,1)	(2,2)	(2,2)	(12,12)
7	(2.00, 2.00)	1.00	(1,1)	(1,1)	(1,1)	(1,1)	(1,1)	(1,1)	(6,6)
8	(1.5, 1.50)	1.00	(1,6.1)	(1,6.1)	(1,6.1)	(1,6.1)	(1,6.1)	(1,6.1)	(6, 36.6)
9	(1.35, 1.50)	0.70	(1,10 ⁻⁹)	(1,10 ⁻⁹)	(1,6.1)	(1,6.1)	(1,12.2)	(1,12.2)	(6, 36.6)

475 **Table 1.** Detail information of the BC particles shown in Fig.2476 ^{*1} Mass of the BC component of and non-BC component (arbitrary unit).